INTERNATIONAL JOURNAL OF CLIMATOLOGY
Int. J. Climatol. (2012)
Published online in Wiley Online Library
(wileyonlinelibrary.com) DOI: 10.1002/joc.3508

Predictability of dry season reforecasts over the tropical and the sub-tropical South American region

Adam Frumkin[a,b]* and Vasubandhu Misra[a,b]

[a] *Department of Earth, Ocean and Atmospheric Science, Florida State University, Tallahassee, FL 32306, USA*
[b] *Center for Ocean-Atmospheric Prediction Studies, Florida State University, Tallahassee, FL 32306, USA*

ABSTRACT: In this study, we diagnose the fidelity of South American dry season (June–July–August) reforecasts from a global climate model (GCM) and a regional climate model (RCM). This includes a set of downscaled integrations of the RCM that uses a bias correction method called anomaly nesting, which is designed to remove the bias of the GCM that forces the RCM at the lateral boundaries. The models are integrated for seven dry seasons (2001–2007), and each season consists of six ensemble members. For this study, we focus on two primary regions: the Amazon River Basin (ARB) and the subtropical (ST) region.

The paper discusses the regions of model bias for 2 m air temperature and for precipitation within ARB and ST regions first using corresponding independent observations and then with the NCEP Climate Forecast System Reanalysis (CFSR). The paper also dwells on the predictability of the above normal, normal and below normal occurrences of the two variables using signal-to-noise ratios and calculation of the area under the relative operative characteristic (ROC) curve (AUC). The models produced the largest biases of both variables over elevated terrain and within the intertropical convergence zone (ITCZ). Signal-to-noise ratios show that the models exhibit more predictability in ARB than they do in ST and that there is more predictability for surface air temperature than for precipitation. AUCs confirm that temperature is more skilfully predicted than precipitation and that the models exhibit more skill in ARB than in ST. AUCs also show that the anomaly nesting integrations have a limited advantage over the rest with some modest improvements in skill of surface temperature prediction over ARB.

Lastly, we evaluate how the three models depict land-atmosphere interactions during the dry season and compare their results with CFSR. We find conflicting results between the global and regional model predictions and CFSR on the relative coupling strength between the land and the atmosphere during the dry season. Copyright © 2012 Royal Meteorological Society

KEY WORDS predictability; Amazon; land–atmosphere coupling

Received 17 May 2011; Revised 7 March 2012; Accepted 3 April 2012

1. Introduction

The tropical South American region exhibits a distinct seasonal cycle of rainfall (Zhou and Lau, 1998; Vera *et al*., 2006; Misra, 2008) like many other monsoon regions of the globe. Raia and Cavalcanti (2008) identified the onset of the South American monsoon for the majority of the monsoon region to be in mid-to-late October and the demise to be in late March. The onset in the northwest regions of the continent occurs in mid-to-late August and moves towards the southwest over time (Vera *et al*., 2006). A weakening and an eastward displacement of the South Atlantic subtropical high accompany the onset period (Vera *et al*., 2006). As a result, the wind field over extreme south-western Amazonia shifts from northerlies to northwesterlies, and over eastern Brazil the winds shift from easterlies to northeasterlies. These changes allow for enhanced moisture transport from Amazonia and the South Atlantic Ocean into the monsoon region (i.e. central South America).

The demise period exhibits an increase in sea level pressure (SLP) over the continent, an easterly moisture flux towards the Amazon region, a reduction in the northerly flow east of the Andes and a reduction in vertical motions. These features primarily result from the seasonal westward shift of the South Atlantic subtropical high (SASH). With the progression of the season to boreal summer, heating over the elevated terrain weakens, the Chaco low weakens, the thermal gradient between the land and the ocean is reduced and the SASH shifts to the west (Zhou and Lau, 1998). Raia and Cavalcanti (2008) noted that during JJA, when many regions of SA experience a minimum in precipitation, there is southeasterly moisture transport over Northeast Brazil driven by the subtropical high. In addition, in austral winter, there is an intense westward moisture transport over the Amazon region, which, because it lacks a southerly component, reduces the moisture transport to regions that typically experience the monsoonal cycle of rainfall.

* Correspondence to: A. Frumkin, Department of Earth, Ocean and Atmospheric Science, Florida State University, Tallahassee, FL 32306, USA. E-mail: vmisra@fsu.edu

One source of motivation for this research is the important role that conditions in the Amazon rainforest during the dry season may play in initiating the wet phase of the SAM (Fu and Li, 2004; Li and Fu, 2004). Myneni *et al*. (2007) showed that changes in leaf area (LA) within the Amazon rainforest are strongly correlated with the seasonal cycle of precipitation and solar radiation. Unlike many other types of forests, which see an increase in LA during the wet season, the Amazon rainforest experiences a 25% increase in leaf area index (LAI) (relative to the wet season) over 60% of its area during the dry season. This increase in LAI is primarily driven by the increased amount of incoming solar radiation that accompanies the decrease in cloud cover during the transition from the wet to the dry season. Myneni *et al*. (2007) suggested that the increase in LA during the dry season eventually leads to the initiation of the wet season; as LA increases, the amount of evapotranspiration and low-level moisture also increases. Increasing the amount of low-level moisture destabilizes the atmosphere and increases the probability of convection occurring towards the end of the dry season.

A second source of motivation for studying the dry phase of the SAM comes from the relationship it may have with the size and intensity of the Atlantic Warm Pool (AWP; Wang and Enfield, 2001; Wang, 2002; Misra and DiNapoli, 2012). Wang (2002) suggested that Amazonian convective activity provides a cross-hemispheric connection to the North Atlantic subtropical high through a Hadley-type circulation. Misra and DiNapoli (2012) suggest that ENSO manifestation on the AWP is through its influence on the atmospheric meridional overturning circulation emanating from the Amazon. The AWP plays a significant role in controlling the occurrence and intensity of Northern Hemisphere phenomena such as Atlantic hurricanes, the Great Plains low-level jet (GPLLJ) and the Caribbean low-level jet (CLLJ). An anomalously large (small) AWP weakens (strengthens) the GPLLJ, weakens (strengthens) the CLLJ and reduces (increases) the tropospheric wind shear in the maximum development region of Atlantic hurricanes, thereby increasing (decreasing) the likelihood of cyclone development (Wang *et al*., 2008).

This study investigates the implications of downscaling the National Centers for Environmental Prediction (NCEP) coupled Climate Forecast System (CFS; Saha *et al*., 2006) over South America (SA), using the NCEP–Scripps Regional Spectral Model (RSM; Kanamitsu and Kanamaru, 2007). In this study, we also evaluate the effect of applying a bias correction process to the GCM before the downscaling is performed with the RCM. The bias correcting process used in this study is referred to as anomaly nesting (AN) (Misra and Kanamitsu, 2004). Hereafter, the RSM integration with the anomaly nested bias correction is referred to as RSM-AN. In this study, we focus on verifying the reforecasts produced for June, July and August (2001–2007) by three models (CFS, RSM and RSM-AN). We also examine the predictability over the adjoining subtropical South American region as our previous austral summer seasonal predictability study (Misra, 2004) showed distinct differences from the predictability over the tropical South American region.

The appeal of AN stems from its attempt to reduce the influence of the systematic errors of the large-scale model that is otherwise forced on the integration of the regional climate model through the lateral boundaries. Misra and Kanamitsu (2004) showed some improvement in seasonal prediction of the SAM using an anomaly nested RCM even when the GCM that was used to force the RCM was strongly biased. Chan and Misra (2011) found that a major benefit of downscaling and AN was in the dynamical fields such as winds, particularly those associated with the low-level jets. This improvement can be at least partially attributed to the higher resolution of the topography in the RCM.

Section 2 describes the models used in this study followed by a description of the model experiments. The results are discussed in Section 4, and the conclusions are discussed in Section 5.

2. Model description

The NCEP CFS is a fully coupled land–ocean–atmosphere dynamical seasonal weather prediction model (Saha *et al*., 2006). The version of the CFS used in this study has 64 vertical sigma levels and is run at a triangular spectral truncation of T62 (∼200 km Gaussian grid). It uses the Simplified Arakawa-Schubert (SAS) cumulus convection (Hong and Pan, 1998), the NCEP Medium Range Forecast (MRF) planetary boundary layer (PBL) scheme (Hong and Pan, 1996) and the Oregon State University land surface scheme (Mahrt and Pan, 1987). Six ensemble members are generated for each integration of the CFS, providing us with 42 total integrations. The ensemble members are generated by perturbing the initial state of the atmosphere following Kirtman *et al*. (2001) and Misra (2004).

Since its release, numerous changes have been made to the NCEP Scripps RSM (Juang *et al*., 1994; Kanamitsu and Kanamaru, 2007). The most pertinent to this study are the updates to the model physics, including scale-selective bias correction (SSBC; Kanamaru and Kanamitsu, 2007). The RSM used in this study has 28 pressure sigma vertical levels and a 60 km horizontal resolution (a significantly coarser resolution than the RSM is typically run at). We use the 60 km resolution because the model was run over a very large domain (North America and South America). The RSM uses the same cumulus (SAS) and PBL parameterizations that are used in the CFS. However, it uses a different land surface scheme, the NCEP-Ohio State-US Air Force-NWS Hydrology Laboratory (NOAH) land scheme (Ek *et al*., 2003).

A second integration of the RSM is performed using AN (Misra and Kanamitsu, 2004). The process of AN refers to the concept of removing the bias of the GCM before downscaling. This is accomplished by replacing the model climatology with the corresponding

climatology from the reanalysis. For this study, the climatology of the CFS JJA atmospheric state variables and SST is replaced with the climatology from the NCEP-NCAR Reanalysis I (Kalnay *et al*., 1996) and ERSSTv2 SST, respectively. Bias corrections are applied to humidity, divergence, vorticity and temperature at all vertical levels of the RSM (Chan and Misra, 2011).

The primary validation data used in this study are acquired from the NCEP Climate Forecast System Reanalysis (CFSR; Saha *et al*., 2010). CFSR is used to locate areas of significant model biases in precipitation and temperature. CFSR is also used to analyse model skill and to locate errors in the land-atmosphere feedbacks in the models. In addition, the Tropical Rainfall Measuring Mission (TRMM) 3B-43 and CPC Merged Analysis (CMAP; Xie and Arkin, 1997) precipitation data sets are also used to evaluate model bias and model skill.

3. Description of model experiments

Three model integrations are conducted for June–September, 2001–2007. All model integrations are started at 0000Z 23 May 2001. Only data corresponding to the South American dry season (June, July and August) are used in this study. Each seasonal integration has six ensemble members. The experiments are named as follows:

1. CFS: Uses the NCEP CFS (Saha *et al*., 2006).
2. RSM: Uses the NCEP Scripps RSM (Kanamitsu and Kanamaru, 2007).
3. RSM-AN: Same as 2 except that the AN procedure is applied to the NCEP CFS data before the downscaling is performed (Misra and Kanamitsu, 2004).

The large-scale area of interest for this study is in the South American continent between 15 N and 40 S and between 30 W and 90 W. Two regions are of particular interest: the ARB and the ST region (Figure 1). ARB is defined as the region between 4 N and 17 S and between 45 W and 75 W. ST is defined as the region between 17 S and 36 S and between 56 W and 68 W. It is also seen from this figure that the coastlines and the orography of the Andes are defined better in the relatively higher resolution of the RSM and RSM-AN compared to CFS.

In the two regions of interest, we analyse the model integrations for their large-scale biases, their seasonal predictability and their skill at predicting 2 m air temperature and precipitation. Lastly, we analyse the land–atmosphere feedbacks in the three integrations to possibly understand the discrepancy between the model reforecasts.

Predictability is analysed following Kumar and Hoerling (1995) using the ratio of signal to total variance (the total variance equals the signal plus the noise) for 2 m air temperature and precipitation (for details, see Appendix I). However, large ratios do not *necessarily* mean that forecasts will be skilful; thus, it is insightful to examine the fidelity of the models further using a probabilistic skill score such as the relative operative characteristic (ROC) curve (Mason and Graham, 1999).

Lastly, we also examine the land–atmosphere feedbacks in the models and compare their results with the corresponding feedbacks in CFSR.

4. Results

4.1. Model bias

In this section, we compare the models' JJA 2001–2007 average precipitation rates to TRMM and CMAP precipi-

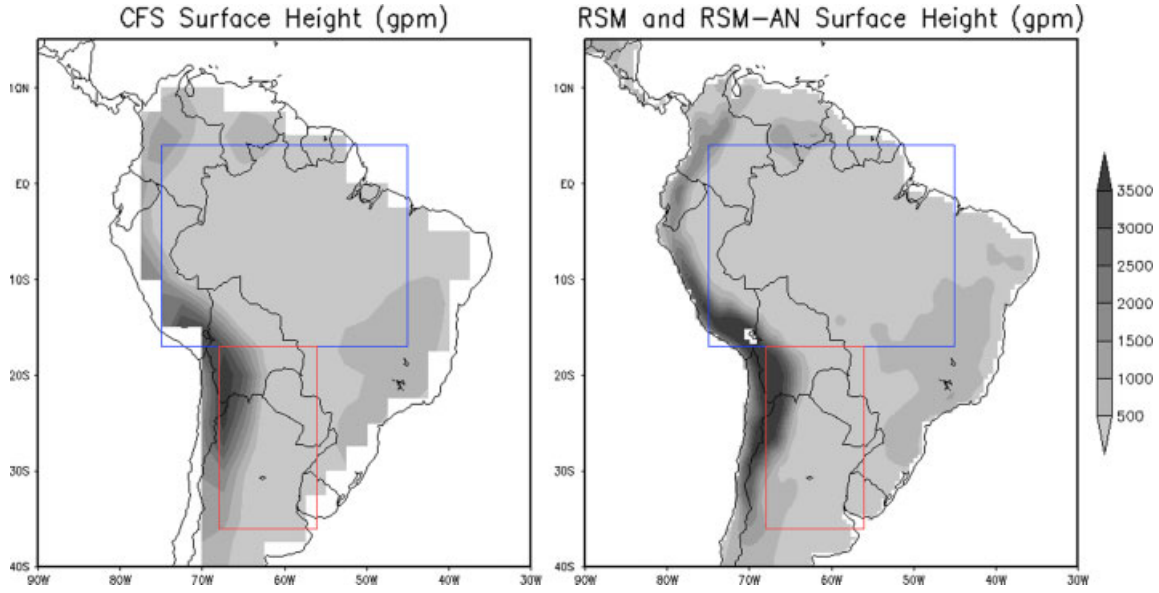

Figure 1. The land area (shaded) and topography (GPM) for the NCEP CFS (a) and the NCEP Scripps RSM (b; and RSM-AN). The blue box represents the Amazon River Basin (ARB), and the red box represents the subtropical (ST) region. This figure is available in colour online at wileyonlinelibrary.com/journal/joc

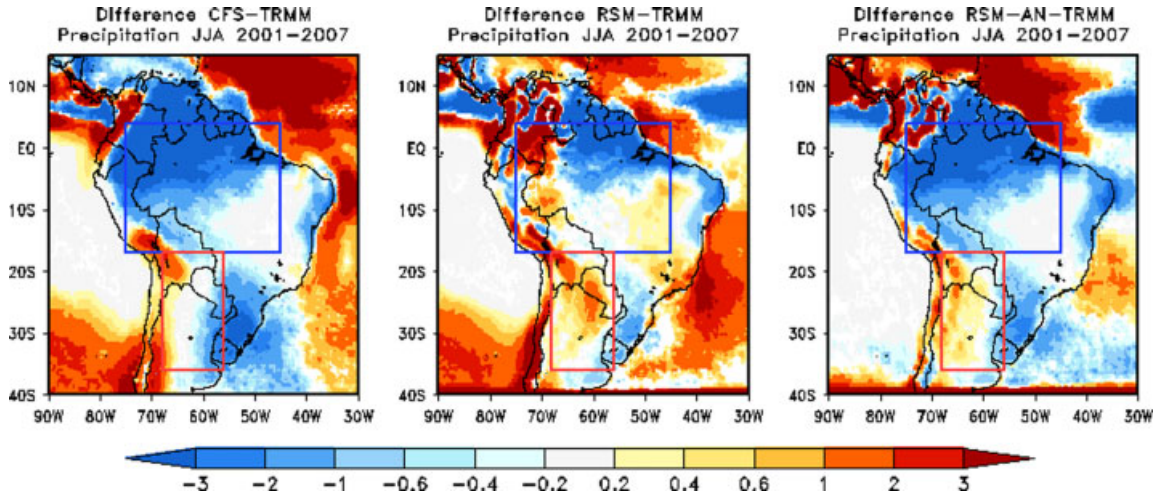

Figure 2. Difference between the JJA 2001–2007 average precipitation rates for the models and TRMM. CFS minus TRMM is on the left, RSM minus TRMM is in the middle and RSM-AN minus TRMM is on the right. The differences are computed by interpolating to the higher resolution grid of TRMM. Units are in millimetre per day. Positive differences indicate that the model rains more than TRMM. Regions that do not meet the 95% confidence level of the Student's *t*-test are masked out in white. This figure is available in colour online at wileyonlinelibrary.com/journal/joc

tation rates and we compare the model's JJA 2001–2007 -metre air temperatures to those of CFSR.

When compared to TRMM precipitation rates (Figure 2), the CFS and RSM-AN precipitation rates are primarily negatively biased within ARB, except over elevated terrain. The RSM exhibits a positive bias over western ARB with negative bias over the northeastern side of ARB. Over ST, the CFS and the RSM-AN display similar patterns of bias: negative bias in the eastern half of the box over the lowlands of Argentina and positive bias in the western half of the box over the Andes Mountains. The RSM is mostly positively biased over ST.

A similar pattern of bias is observed when the three models are compared to CMAP (Figure 3). Although the positive bias in the northwestern edge of the ARB is relatively diminished compared to the differences with the TRMM data sets (Figure 2). In Figure 3, the CFS and RSM-AN are negatively biased over ARB and ST. When compared to both TRMM and CMAP, the RSM displays similar patterns of positive and negative bias in ARB and ST. The results of the comparisons with TRMM and CMAP indicate that the models are generally negatively biased in ARB, with the RSM having the smallest bias of the three models and in some instances actually exhibiting a positive bias. Over ST, all three models are positively biased over the Andes Mountains and negatively biased over the lower terrain of Argentina.

The models' JJA 2001–2007 two-metre temperature field is compared to the same field from CFSR only. Figure 4 shows that the RSM temperature field is most similar to CFSR temperature field. In ARB, the RSM has a bias of ∼0.01 C, whereas the CFS and RSM-AN exhibit positive biases of 3.5 and 0.9 C, respectively. In ST, the CFS and RSM-AN no longer exhibit the same

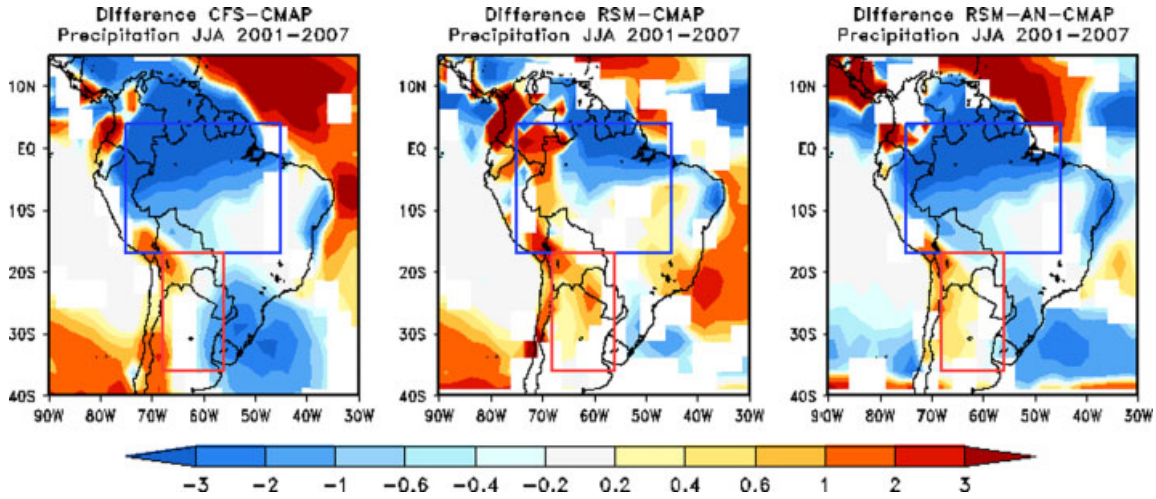

Figure 3. Difference between the JJA 2001–2007 average precipitation rates for the models and CMAP. CFS minus CMAP is on the left, RSM minus CMAP is in the middle and RSM-AN minus CMAP is on the right. The differences are computed by interpolating to the grid of CMAP. Units are in millimetre per day. Positive differences indicate that the model rains more than CMAP. Regions that do not meet the 95% confidence level of the Student's t -test are masked out in white. This figure is available in colour online at wileyonlinelibrary.com/journal/joc

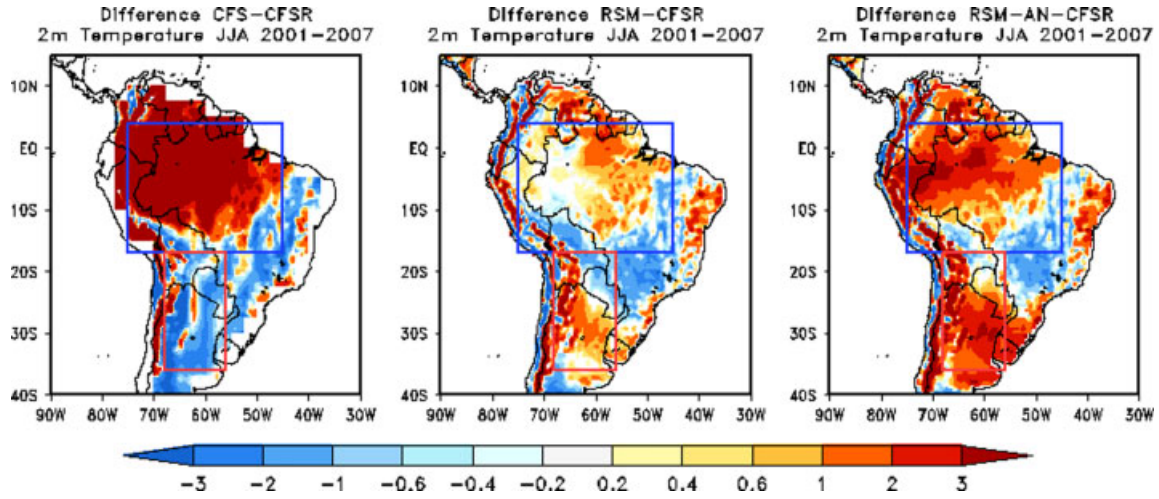

Figure 4. Difference between the JJA 2001–2007 average 2 m air temperature between the models and CFSR. CFS minus CFSR is on the left, RSM minus CFSR is in the middle and RSM-AN minus CFSR is on the right. The differences are computed by interpolating to the grid of CFSR. Units are in 0C. Regions that do not meet the 95% confidence level of the Student's t -test are masked out in white. Additionally the differences over ocean are not shown. Grid boxes over water are masked out. This figure is available in colour online at wileyonlinelibrary.com/journal/joc

pattern. Here, the CFS is negatively biased (∼−1.5 C), whereas the RSM (∼0.6 C) and RSM-AN (2.1 C) are both mostly positively biased. As we can see, the RSM, again, has the smallest bias. Our results suggest that the RSM-AN potentially retains more of the CFS's bias than the RSM does, particularly over ARB.

4.2. Signal-to-noise ratio

The seasonal predictability stems from the fact that atmospheric anomalies are largely governed by boundary condition such as SST anomalies (Shukla, 1998). By comparing the ratio of the variance of the external forcing to the total variance, we can arrive at a measure of the predictability within the modelling system. Larger ratios mean that the system has high predictability, whereas smaller ratios mean that the internal variance of the model is overwhelming the signal from the boundary conditions. It is important to point out that a higher predictability in any given location does not necessarily mean that the model will have more skill in that region as well.

Figure 5 shows the ratio of the signal to the total variance of the mean JJA precipitation for the three models. The models display scattered regions of ratio values >0.5 in ARB and in ST. However, the CFS and the RSM display some areas of larger ratio values in the northern and eastern portions of ARB, whereas the RSM-AN displays higher values of the ratio in the northern portion only. There are almost no values >0.5 in ST in any of the models. The spotty areas of higher predictability observed in ARB seem to coincide with regions of high topography or within the intertropical convergence zone (ITCZ).

All of the models display larger ratios in ARB for 2 m temperature than they do for precipitation (Figure 6). However, there is comparatively less predictability of the 2 m air temperature over ST in all of the model

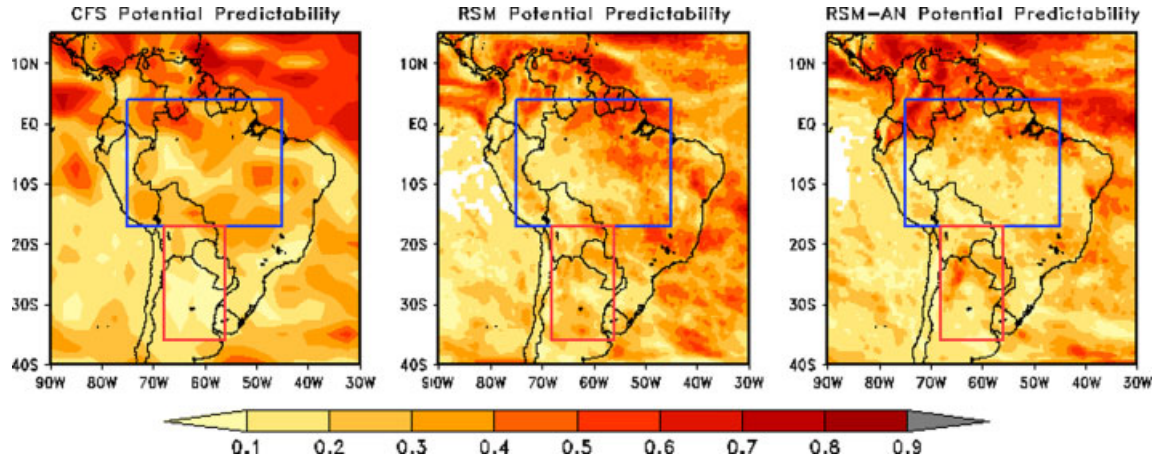

Figure 5. The ratio of the signal to the total variance or, predictability, for the six ensemble members from 2001 to 2007. CFS is on the left, the RSM is in the middle and the RSM-AN is on the right. In the RSM and RSM-AN, regions in the western Pacific Ocean that show up in white are areas where the model did not produce any precipitation and the calculation of the predictability was undefined. This figure is available in colour online at wileyonlinelibrary.com/journal/joc

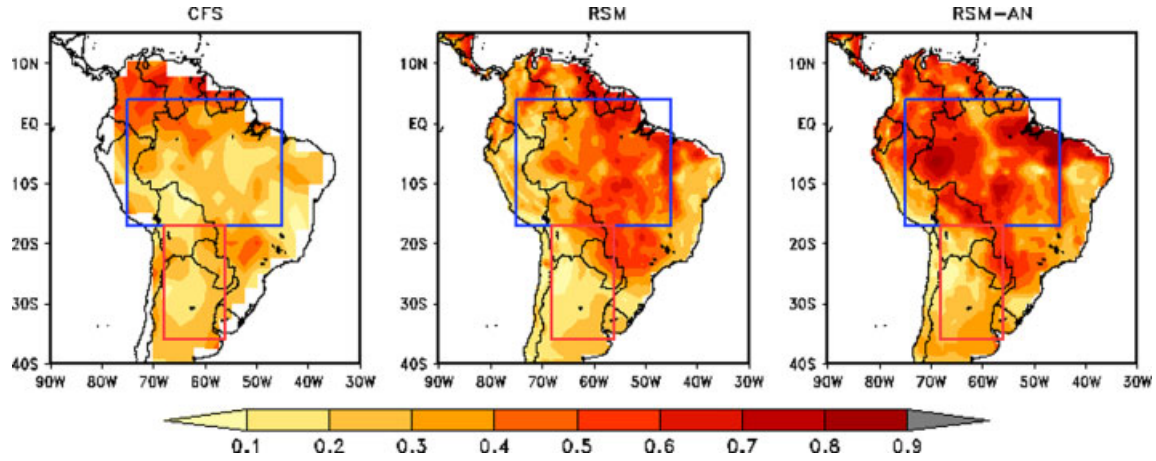

Figure 6. The ratio of the signal to the total variance or predictability of 2 m air temperature, for the six ensemble members from 2001 to 2007. CFS is on the left, the RSM is in the middle and the RSM-AN is on the right. Predictability over the oceans is not shown. This figure is available in colour online at wileyonlinelibrary.com/journal/joc

hindcasts compared to that over ARB. The RSM and the RSM-AN display larger ratios than the CFS in both ARB and ST. Over ST, the CFS does not display any values >0.5, whereas the RSM and RSM-AN show some relative increase in predictability especially in the northeast corner of ST. As discussed in Section 3.1, the CFS 2 m air temperature field also exhibits the largest bias when compared to CFSR's temperatures. Although large bias does not necessarily mean low predictability or low ensemble forecast skill, it could, in many instances, be an early indicator of such a problem. A way to get a measure of the model's ensemble forecasting skill is to calculate the area under the ROC curve, which is discussed in Section 3.3.

4.3. Model skill

There are two primary objectives we hope to achieve through our ROC curve analysis. First, we would like to know if any of the three models possess some skill (i.e. AUC > 0.5) in predicting below normal, normal or above normal seasonal mean temperature and precipitation anomalies. The three aforementioned conditions are referred to as *events* throughout this study. Second, we wish to determine if either the downscaling process or the AN process improves the skill of the forecasts. These objectives with regard to precipitation are discussed in Section 4.3.1 and in Section 4.3.2 with regard to temperature.

The results of the AUC calculations are illustrated in Figures 7–10. Generally, the models display higher forecast skill in ARB than they do in ST, and temperature forecasts are more skilful than precipitation forecasts. This corresponds well with the results from Section 4.2; recall that temperature had more predictability than precipitation and that ARB had more predictability than ST.

4.3.1. Precipitation

Using CMAP as the validation data set, the RSM-AN displays the highest skill of the three models for above and below normal events over ARB (Figure 7). For normal events, RSM is the only model that shows any skill. However, over ST (Figure 8), the results are more sobering with RSM exhibiting some nominal skill for below

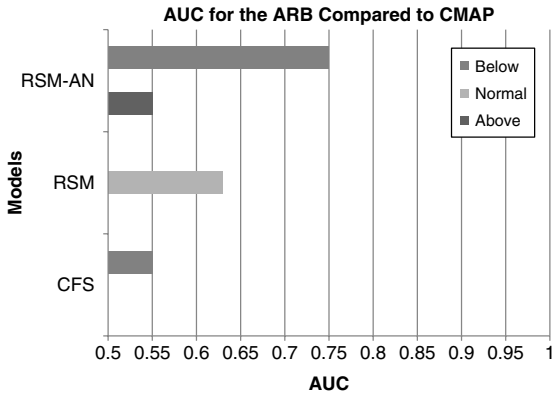

Figure 7. Bar graph depicting the area under the ROC curves calculated for above normal, normal and below normal precipitation events using CMAP as the validation data set for ARB. The three primary models (CFS, RSM and RSM-AN) are shown. Only AUCs >0.5 are shown because values less than that indicate that the model has no skill.

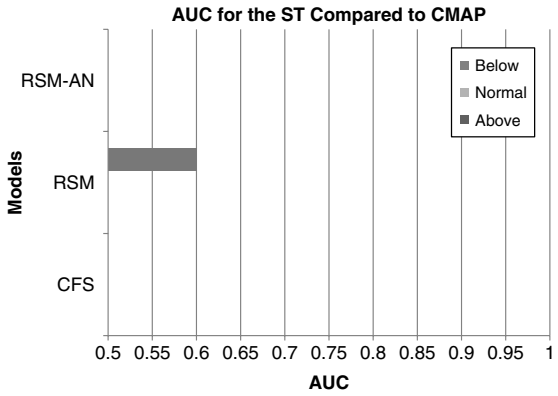

Figure 8. Bar graph depicting the area under the ROC curves calculated for above normal, normal and below normal precipitation events using CMAP as the validation data set for ST. The three primary models (CFS, RSM and RSM-AN) are shown. Only AUCs >0.5 are shown because values less than that indicate that the model has no skill.

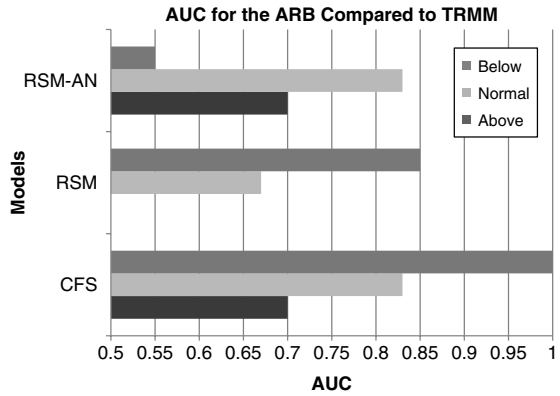

Figure 9. Bar graph depicting the area under the ROC curves calculated for above normal, normal and below normal precipitation events using TRMM as the validation data set for ARB. The three primary models (CFS, RSM and RSM-AN) are shown. Only AUCs >0.5 are shown because values less than that indicate that the model has no skill.

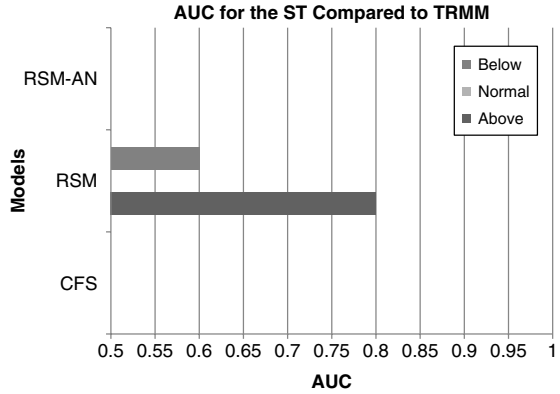

Figure 10. Bar graph depicting the area under the ROC curves calculated for above normal, normal and below normal precipitation events using TRMM as the validation data set for ST. The three primary models (CFS, RSM and RSM-AN) are shown. Only AUCs >0.5 are shown because values less than that indicate that the model has no skill.

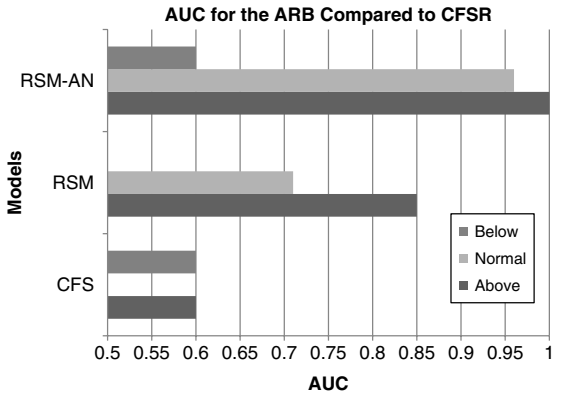

Figure 11. Bar graph depicting the area under the ROC curves calculated for above normal, normal and below normal 2 m air temperature events using CFSR as the validation data set for ARB. The three primary models (CFS, RSM and RSM-AN) are shown. Only AUCs >0.5 are shown because values less than that indicate that the model has no skill.

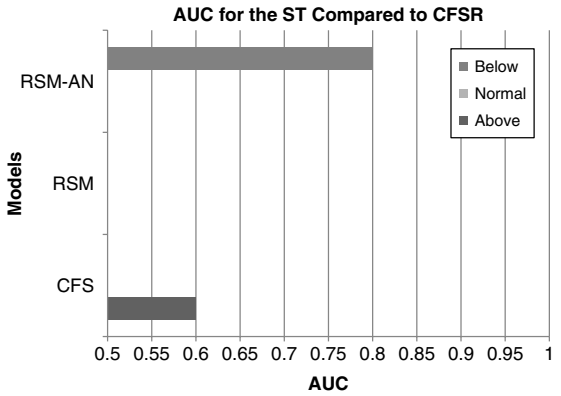

Figure 12. Bar graph depicting the area under the ROC curves calculated for above normal, normal and below normal 2 m air temperature events using CFSR as the validation data set for ST. The three primary models (CFS, RSM and RSM-AN) are shown. Only AUCs >0.5 are shown because values less than that indicate that the model has no skill.

normal events, while the other two models exhibit no skill. In using TRMM as a validation data set, the prediction skill results of the models change (Figures 9 and 10). It now appears that CFS is the most skilful over ARB for all events followed by RSM. Over ST, only RSM displays some reasonable skill for below and above normal events. The fact that these skill measures of the model changes with the validation data sets highlights the complexity of measuring the skill scores of models objectively. In the case of ROC curves, the exact value of the forecast by the model for a particular year is not of utmost importance. Rather, whether that value is above or below normal relative to other years in the model and whether that ranking matches the ranking given to that same year by the validation data set takes precedence.

4.3.2. Two-meter temperature

To estimate the model skill for above normal, normal and below normal temperature events, we calculate ROC curves using CFSR 2 m air temperature as the validation data set. In ARB, the RSM-AN has the most skill predicting all three events (Figure 11). The RSM has the next highest skill for normal and above normal temperature events, although it has no skill predicting below normal events. The CFS has the least skill predicting normal and above normal events, but unlike the RSM it exhibits some skill predicting below normal events. It is interesting to note that contrary to larger climatological errors in RSM-AN compared to RSM over ARB (Figure 4), the skill of the seasonal prediction anomalies of the 2 m air temperature from RSM-AN exceeds that from RSM.

Over ST, the results are far less definitive. The CFS displays some skill forecasting above normal events only, the RSM-AN displays relatively higher skill forecasting below normal events only and the RSM displays no skill with any of the events (Figure 12).

4.4. Land–atmosphere feedbacks

The final aspect of this study is to determine how the land and the atmosphere interact in the three models,

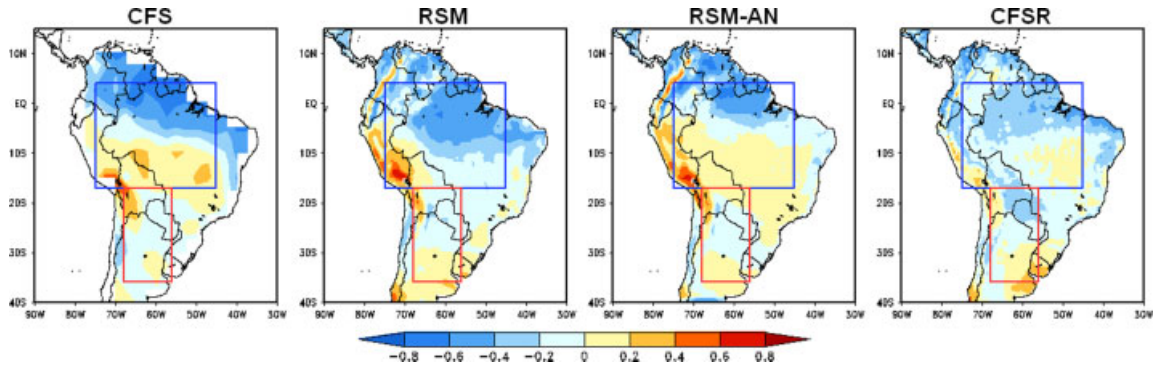

Figure 13. Contemporaneous correlation between temperature and precipitation for the three models and for CFSR. This figure is available in colour online at wileyonlinelibrary.com/journal/joc

to try explaining the differences in seasonal predictability amongst the models. Koster *et al*. (2003) split the land–atmosphere feedback into three parts (described in terms of wet anomalies): (1) wetting of soil by precipitation, (2) enhancement of evaporation by the wet soil, and (3) enhancement of precipitation by evaporation. Part (1) is obvious. Part (2) can be supported by contemporaneous correlations of temperature and precipitation, which, in terms of wet anomalies, would be negative. The argument being that higher precipitation leads to more evapotranspiration, which in turn leads to lower temperatures (Koster *et al*., 2003). The third part of the feedback is more debatable, partly due to limited observations. In addition, it is difficult to determine causality between a set of variables, which are highly interconnected (Misra and Dirmeyer, 2009). As a result, we can at best hope to offer a qualitative diagnostic of this part of the feedback cycle. To investigate this third part, we follow Misra and Dirmeyer (2009) and calculate contemporaneous correlation coefficients between two pairs of variables: (1) evaporation and precipitation and (2) downwelling short wave flux and evaporation. Appendix II lists all three variable pairings we have just discussed and describes the information that can be inferred from the results. We conduct the three sets of correlations for each of the three models and compare the results with the same set of correlations from CFSR in an attempt to locate errors in the models.

As discussed, the second part of the land–atmosphere feedback can be illustrated with contemporaneous correlations between precipitation and temperature. This correlation over northern portion of ARB is largely negative, while the southern parts of the ARB display a weak positive correlation across all models and CFSR (Figure 13). However, there are subtle differences, such as the far limited extent of the negative correlation in RSM-AN over north ARB and more extensive distribution of the positive correlation in south ARB. On the other hand, RSM shows a more widespread negative correlation between precipitation and temperature over ARB and very narrow extent of the positive correlation on the western edge of the ARB. Notwithstanding these subtle differences, the large-scale distribution of these correlation patterns imply that in the northern portion of the ARB, precipitation is recycled, that is wetting the soil, and then being evaporated back into the atmosphere. In the southern ARB, the results suggest that surface evaporation is not leading to precipitation. In ST, correlations are very weak with no distinct spatial pattern.

The third part of the cycle, the enhancement of precipitation by evaporation, is explained by the last two sets of correlations. All three models exhibit positive correlations between downwelling short wave flux and evaporation both over ARB and over ST (Figure 14). This indicates that in SA during the dry season, evaporation is energy limited. The term energy limited implies that evaporation from the surface is limited by the amount

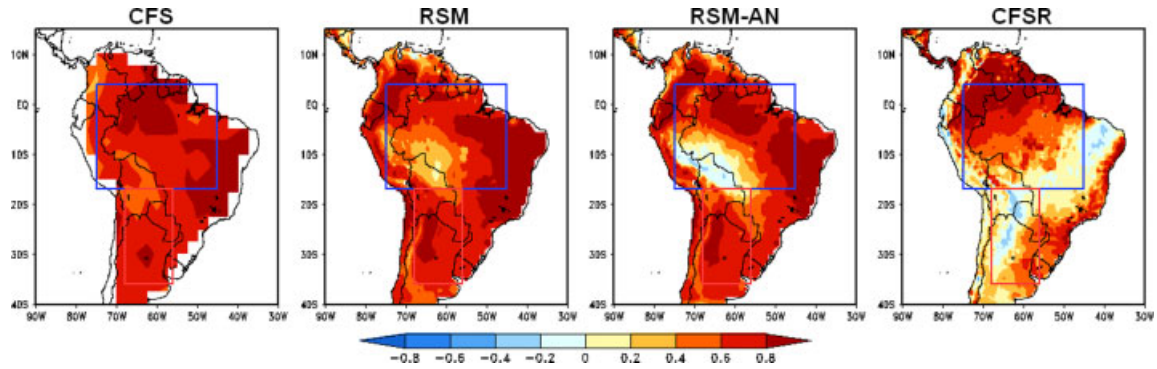

Figure 14. Contemporaneous correlation between downwelling short wave flux and evaporation for the three models and for CFSR. This figure is available in colour online at wileyonlinelibrary.com/journal/joc

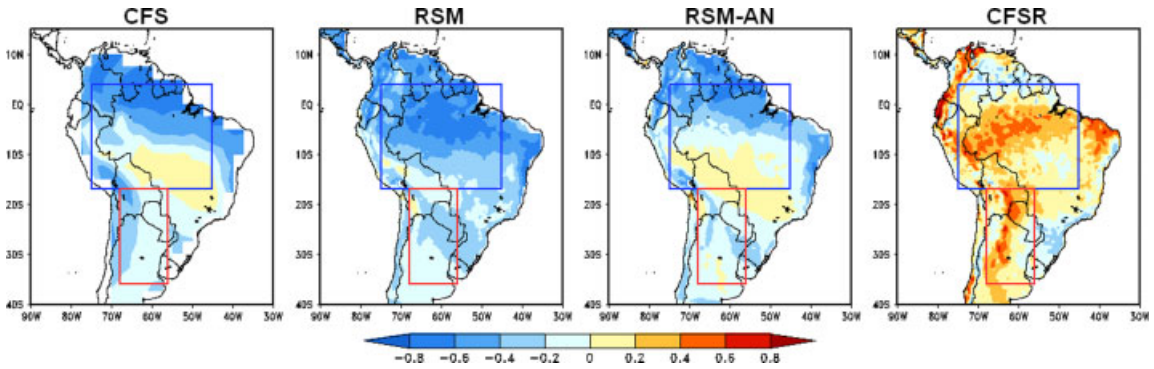

Figure 15. Contemporaneous correlation between evaporation and precipitation for the three models and for CFSR. This figure is available in colour online at wileyonlinelibrary.com/journal/joc

of downwelling short wave flux. This result is consistent with the negative correlations between evaporation and precipitation (Figure 15).

Spatially the correlations of evaporation with precipitation are relatively similar to correlations of temperature with precipitation. However, RSM does show a dominance of the negative correlations over SA unlike CFS and RSM-AN that show weak positive correlations in southern ARB. Negative values are a mark of a wet climate, with remote moisture sources being the likely dominant factor for local precipitation. This result, however, conflicts with our interpretation of the correlations between temperature and precipitation. From that plot, we concluded that cooling from surface evaporation during precipitation leads to temperature decreasing when precipitation increases. So in essence, this analysis suggests that the model is evaporating weakly from a wet soil as a result of insufficient incoming solar radiation.

4.4.1. CFSR

When the same sets of correlations are performed with CFSR, the results are similar to those obtained from the suite of models. Figure 13 shows that the correlation pattern between temperature and precipitation is spatially similar to the pattern produced by the models. It shows negative correlations in the northern portion of ARB and weak positive values in the southern portion. These results indicate that evaporation probably fuels precipitation in the northern part of ARB but not in the southern portion. Correlation coefficients in ST region are a mix between weak positive and weak negative values. As was the case in the models, CFSR shows mostly positive correlations between downwelling short wave flux and evaporation in ARB, meaning evaporation is energy limited (Figure 14). In ST, however, there is a small region where correlations are negative; thus, evaporation is moisture limited. The largest differences between the models and CFSR occur in the correlations of evaporation and precipitation (Figure 15). Unlike the models, CFSR shows primarily positive correlations between these variables in both ARB and ST. This means that CFSR is indicating that SA in austral winter is in an arid regime, whereas the models are suggesting that SA is in a wet regime.

5. Conclusions

In this study, we analysed the output of three climate model integrations, the NCEP CFS, the NCEP Scripps RSM and the NCEP Scripps RSM with bias correction applied to the CFS data, for seven dry seasons of the South American monsoon.

We found that all three models, when compared to CFSR, exhibited positive biases of 2 m air temperature in ARB (tropical region of the domain), where the CFS possessed the largest bias. In ST (subtropical region of the domain), the CFS was negatively biased, whereas the RSM and the RSM-AN were positively biased.

Model differences were found in the seasonal predictability over ARB and in ST. In all models, both precipitation and 2 m air temperature, ARB exhibited larger predictability than did ST. The study also indicated that the models had higher predictability for temperature than for precipitation, particularly over ARB. However, predictability of a model is not necessarily indicative of a model's skill. Although, in this study, we found that the seasonal predictability for austral winter was a fair first approximation of model skill over ARB and ST regions.

When analysing 2 m air temperature, we found it most beneficial to apply the downscaling and AN processes in both regions.

The same conclusions were reached using CMAP as a validation data set. Interestingly, when using TRMM as our validation data set, we found no added benefit to applying either the downscaling or the AN methods in ARB, but our conclusions for ST were identical to those reached when we used CFSR and CMAP.

The investigation into land–atmosphere interactions in the models and in CFSR provided some insight to the skills displayed by the models. The land–atmosphere feedback analysis in CFSR suggests that most of the tropical and subtropical SA is in an arid regime during austral winter, whereas the model seasonal hindcasts suggest that it is in a humid regime. This difference is striking in the correlations between evaporation and precipitation with models and CFSR showing largely negative values and positive values, respectively. This analysis implies that remote sources of moisture contribute more substantially in the model hindcasts than in CFSR.

This study suggests that validation of model seasonal hindcasts over South America is a difficult task especially when validating precipitation forecasts. The difference in the results using CMAP and TRMM in this study is suggestive of such a conclusion. This difference can partially be attributed to difference in the resolutions of the two validation data sets. Furthermore, this study is unable to detect any possible relationship between the seasonal prediction skill of the models and its climatological errors. There are instances when the climatological errors are large (small) and the seasonal hindcast skill is relatively small (large).

Acknowledgements

The authors acknowledge the help of Mr Steven DiNapoli of the Center for Ocean-Atmospheric Prediction Studies, Florida State University, for his assistance with the figures. This work was supported by NOAA grant NA07OAR4310221. Its contents are solely the responsibility of the authors and do not necessarily represent the official views of the acknowledged funding agencies. We also acknowledge the support of the FSU high-performance computing center (http://www.hpc.fsu.edu/), where the model integrations were completed.

Appendix I

For this study, there will be $M = 6$ ensemble members with $N = 7$ years where the ensemble member is represented by j and the year is represented by i. The ensemble mean for a given climate variable for one model and for 1 year is then

$$\overline{x}_i = \frac{1}{M}\sum_{j=1}^{M} x_{ji}.$$

The internal variance or the spread around the ensemble mean for a particular year is then

$$\sigma_i^2 = \frac{1}{M}\sum_{j=1}^{M}(x_{ji} - \overline{x}_i)^2.$$

However, the spread can be dependent on the choice of year so we average the internal variance over all possible years and the result is referred to as noise.

$$\sigma_{\text{noise}}^2 = \frac{1}{N}\sum_{j=1}^{M}\sigma_i^2$$

The external variance, or the signal, is an estimate of the degree to which the difference between the ensemble mean forecasts or different years is due to boundary conditions rather than to chance (Stefanova *et al*., 2010). The climatological ensemble mean for the particular variable is

$$\overline{x} = \frac{1}{N}\frac{1}{M}\sum_{i=1}^{N}\sum_{j=1}^{M} x_{ji}$$

and the external variance is given by

$$\sigma_{\text{signal}}^2 = \frac{1}{N}\sum_{i=1}^{N}(\overline{x}_i - \overline{x})^2.$$

Finally, the total variance of the system is given by

$$\sigma_{\text{total}}^2 = \sigma_{\text{signal}}^2 + \sigma_{\text{noise}}^2.$$

By comparing the ratio of σ_{signal}^2 to σ_{total}^2, it can be determined which part of the observed signal is due to boundary conditions and which part is due to the uncertainty of the initial conditions. Larger ratios indicate more predictability of the climate variable. Values near one mean that the boundary conditions are overwhelming the effect of the noise and values near zero indicate that the model is not 'seeing' the boundary conditions (i.e. the entire signal is noise; Stefanova *et al*., 2010).

Appendix II

Variable pair	Purpose
Temperature w/Precipitation	Negative correlations suggest that surface evaporative cooling due to precipitation reduces temperatures. Positive correlations suggest that evaporation is not contributing to precipitation (Koster *et al*., 2003).
Evaporation w/Precipitation	Positive correlations indicate an arid climate regime, where precipitation is fed by local evaporative sources. Negative correlations indicate a wet regime (Misra and Dirmeyer, 2009).
Downwelling Short Wave Flux w/Evaporation	Positive correlations indicate an *energy-limited* regime. An energy-limited regime is one in which plentiful moisture exists at the surface to fuel evaporation and evaporation is limited by the amount of radiation that reaches the surface. Negative correlations indicate a *moisture limited* regime, a regime in which evaporation rates are limited by the amount of moisture available at the surface rather than the amount of incoming solar radiation (Misra and Dirmeyer, 2009).

References

Chan SC, Misra V. 2011. Dynamic downscaling of the North American monsoon with the NCEP Scripps regional spectral model from the NCEP CFS global model. *Journal of Climate*. **24**: 653–673.

Ek MB, Mitchell KE, Lin Y, Roger E, Grunmann P, Koren V, Gayno G, Tarpley JD. 2003. Implementation of the upgraded Noah land-surface model in the NCEP operational mesoscale Eta model. *Journal of Geophysical Research* **108**: 8851. DOI: 10.1029/2002JD003296.

Fu R, Li W. 2004. The influence of the land surface on the transition from dry to wet season in Amazonia. *Theoretical and Applied Climatology* **78**: 97–110.

Hong SY, Pan HL. 1996. Nonlocal boundary layer vertical diffusion in a medium-range forecast model. *Monthly Weather Review* **124**: 2322–2339.

Hong SY, Pan HL. 1998. Convective trigger function for a mass-flux cumulus parameterization scheme. *Monthly Weather Review* **126**: 2599–2620.

Juang HM, Kanamitsu M. 1994. The NMC nested regional spectral model. *Monthly Weather Review* **122**: 3–26.

Kalnay E, Kanamitsu M, Kistler R, Collin W, Deaven D, Gandin L, Iredell M, Saha S, White G, Woollen J, Zhu Y, Leetmaa A, Reynolds R, Chelliah M, Ebisuzaki W, Higgin W, Janowiak J, Mo KC, Ropelewski C, Wang J, Roy Jenne, Joseph D. 1996. The NCEP/NCAR 40 year reanalysis project. *Bulletin of the American Meteorological Society* **77**: 437–471.

Kanamaru H, Kanamitsu M. 2007. Scale-selective bias correction in a downscaling of global analysis using a regional model. *Monthly Weather Review* **135**: 334–350.

Kanamitsu M, Kanamaru H. 2007. Fifty-seven year reanalysis downscaling at 10 km (CaRD10). Part I: System detail and validation with observations. *Journal of Climate* **20**: 5553O5 71.

Kirtman BP, Paolino DA, Kinter JL III, Straus DM. 2001. Impact of tropical subseasonal SST variability on seasonal mean climate simulations. *Monthly Weather Review* **129**: 853–868.

Koster RD, Suarez MJ, Higgin RW, Van den Dool HM. 2003. Observational evidence that soil moisture variations affect precipitation. *Geophysical Research Letters* **30**: 1241. DOI: 10.1029/2002GL016571.

Kumar A, Hoerling MP. 1995. Prospects and limitations of seasonal atmospheric GCM predictions. *Bulletin of the American Meteorological Society* **76**: 335–345.

Li W, Fu R. 2004. Transition of the large-scale atmospheric and land surface conditions from the dry to the wet season over Amazonia as diagnosed by the ECMWF re-analysis. *Journal of Climate*, **17**: 2637–2651.

Mahrt L, Pan H-L. 1987. A two-layer model of soil hydrology. *Boundary-Layer Meteorology* **29**: 1–20.

Mason SJ, Graham NE. 1999. Conditional probabilities, relative operating characteristics and relative operating levels. *Weather and Forecasting* **14**: 713–725.

Misra V, DiNapoli S. 2012. The observed teleconnection between the Equatorial Amazon and Intra-Americas seas. *Climate Dynamics*. In review.

Misra V. 2004. An evaluation of the predictability of the austral summer seasonal precipitation over South America. *Journal of Climate* **17**: 1161–1175.

Misra V. 2008. Coupled air, sea, and land interactions of the South American monsoon. *Journal of Hydrometeorology* **21**: 6389–6403.

Misra V, Dirmeyer PA. 2009. Air, sea, and land interactions of the continental US hydroclimate. *Journal of Hydrometeorology* **10**: 353–373.

Misra V, Kanamitsu M. 2004. Anomaly nesting: a methodology to downscale seasonal 8 climate simulations from AGCMs. *Journal of Climate* **17**: 3249–3262.

Myneni RB, Yang W, Nemani RR, Huete AR, Dickinson RE, Knyazikhin Y, Didan K, Fu R, Negron Juarez RI, Saatchi SS, Hashimoto H, Ichii K, Shabanov NV, Tan B, Ratana P, Privette JL, Morisette JT, Vermote EF, Roy DP, Wolfe RE, Friedl MA, Running SW, Votava P, El-Saleous N, Devadiga S, Su Y, and Salomonson VV. 2007. Large seasonal swings in leaf area of Amazon rainforests. *Proceedings of the National Academy of Sciences of the United States of America* **104**: 4820–4823.

Raia A, Cavalcanti IFA. 2008. The life cycle of the South American monsoon system. *Journal of Climate* **21**: 6227–6246.

Saha S, Nadiga S, Thiaw C, Wang J, Wang W, Zhang Q, Van den Dool HM, Pan HL, Moorthi S, Behringer D, Stokes D, White G, Lord S, Ebisuzaki W, Peng P, Xie P. 2006. The NCEP Climate Forecast System. *Journal of Climate* **19**: 3483–3517.

Saha S, Moorthi S, Pan HL, Wu X, Wang J, Nadiga S, Tripp P, Kistler R, Woollen J, Behringer D, Liu H, Stokes D, Grumbin R, Gayno G, Wang J, Hou YT, Chuang HY, Juang HMH, Sela J, Iredell M, Treadon R, Kleist D, Delst PV, Keyser D, Derber J, Ek M, Meng J, Wei H, Yang R, Lord S, van den Dool HM, Kumar A, Wang W, Long C, Chelliah M, Xue Y, Huang B, Higgin W, Zou CZ, Liu Q, Chen Y, Han Y, Cucurull L, Reynolds RW, Rutledge G, Goldber M. 2010. The NCEP Climate Forecast Reanalysis. *Bulletin of the American Meteorological Society* **91**: 1015–1057.

Shukla J. 1998. Predictability in the midst of chaos: a scientific basis for climate forecasting. *Science* **282**: 728–731.

Stefanova L, Misra V, O'Brien JJ, Chassignet EP, Hameed S. 2010. Hindcast skill and predictability for precipitation and two-meter air temperature anomalies in global circulation models over the Southeast United States. *Climate Dynamics* (in press), DOI: 10.1007s00382-010-0988-7.

Vera C, Higgin W, Amador J, Ambrizzi T, Garreaud R, Gochis D, Gutzler D, Lettenmaier D, Marengo J, Mechoso CR, Paegle JN, Silva Dias PL, Zhang C. 2006. Toward a unified view of the American monsoon systems. *Journal of Climate* **19**: 4977–5000.

Wang C. 2002. Atlantic climate variability and its associated atmospheric circulation cells. *Journal of Climate* **15**: 1516–1536.

Wang C, Enfield DB. 2001. The tropical Western Hemisphere warm pool. *Geophysical Research Letters* **28**: 1635–1638.

Wang C, Lee S-K, Enfield DB. 2008. Climate response to anomalously large and small Atlantic warm pools during the summer. *Journal of Climate* **21**: 2437–2450.

Xie P, Arkin PA. 1997. Global precipitation: a 17 year monthly analysis based on gauge observations, satellite estimates, and numerical model outputs. *Bulletin of the American Meteorological Society* **78**: 2539–2558.

Zhou J, Lau K-M. 1998. Does a monsoon climate exist over South America? *Journal of Climate* **11**: 1020–1040.

